Global Biogeochemical Cycles

RESEARCH ARTICLE
10.1029/2019GB006467

A Global Model for Iodine Speciation in the Upper Ocean

Martin R. Wadley[1], David P. Stevens[1], Tim D. Jickells[2], Claire Hughes[3], Rosie Chance[4], Helmke Hepach[5], Liselotte Tinel[4], and Lucy J. Carpenter[4]

[1]School of Mathematics, University of East Anglia, Norwich, UK, [2]School of Environmental Sciences, University of East Anglia, Norwich, UK, [3]Department of Environment and Geography, University of York, York, UK, [4]Department of Chemistry, University of York, York, UK, [5]GEOMAR Helmholtz Centre for Ocean Research Kiel, RD2, Biological Oceanography, Kiel, Germany

Key Points:
- We develop a model for iodine speciation and cycling in the ocean
- The predicted surface iodide distribution has a zonal structure not readily discernable by the limited observations to date
- Ocean circulation is found to have an important role in determining the spatial distribution of iodide

Correspondence to:
M. R. Wadley,
m.wadley@uea.ac.uk

Citation:
Wadley, M. R., Stevens, D. P., Jickells, T. D., Hughes, C., Chance, R., Hepach, H., et al. (2020). A global model for iodine speciation in the upper ocean. *Global Biogeochemical Cycles*, *34*, e2019GB006467. https://doi.org/10.1029/2019GB006467

Received 8 NOV 2019
Accepted 3 JUN 2020
Accepted article online 7 JUL 2020

Abstract An ocean iodine cycling model is presented, which predicts upper ocean iodine speciation. The model comprises a three-layer advective and diffusive ocean circulation model of the upper ocean and an iodine cycling model embedded within this circulation. The two primary reservoirs of iodine are represented, iodide and iodate. Iodate is reduced to iodide in the mixed layer in association with primary production, linked by an iodine to carbon (I:C) ratio. A satisfactory model fit with observations cannot be obtained with a globally constant I:C ratio, and the best fit is obtained when the I:C ratio is dependent on sea surface temperature, increasing at low temperatures. Comparisons with observed iodide distributions show that the best model fit is obtained when oxidation of iodide back to iodate is associated with mixed layer nitrification. Sensitivity tests, where model parameters and processes are perturbed, reveal that primary productivity, mixed layer depth, oxidation, advection, surface freshwater flux, and the I:C ratio all have a role in determining surface iodide concentrations, and the timescale of iodide in the mixed layer is sufficiently long for nonlocal processes to be important. Comparisons of the modeled iodide surface field with parameterizations by other authors show good agreement in regions where observations exist but significant differences in regions without observations. This raises the question of whether the existing parameterizations are capturing the full range of processes involved in determining surface iodide and shows the urgent need for observations in regions where there are currently none.

Plain Language Summary Iodine in the ocean is important because small emissions of iodine species to the atmosphere have a significant impact on ozone and air quality. Iodine is converted between two chemical forms by phytoplankton and bacteria, but only one chemical form (iodide) results in atmospheric emissions. We have developed a model that predicts the amount of each type of iodine in the global oceans. We find that this distribution has a more complex structure than that suggested by the limited number of observations, with the ocean circulation playing an important role. The model improves our understanding of both ocean iodine cycling and the resultant impacts on ozone distribution and air quality and also shows that biological and chemical changes to the oceans due to increased atmospheric greenhouse gas concentrations are likely to result in significant changes in ocean iodine, with implications for atmospheric air quality and global elemental cycles.

1. Introduction

The biogeochemical cycling and speciation of iodine in the oceans has been studied for many years, and it is recognized as a "biointermediate" element cycled between oxidized and reduced forms and removed from surface waters by biological activity (e.g., Truesdale et al., 2000). Recently, there has been increasing interest in understanding this speciation because of its potential utility as an indicator of productivity (e.g., Campos et al., 1996; Ducklow et al., 2018; Tian et al., 1996; Wong, 2001), its application as a paleoredox indicator (e.g., Lu et al., 2016; Zhou et al., 2016), and because reactions between iodide at the sea surface and ozone have been identified as a globally significant sink for tropospheric ozone, with implications for atmospheric chemistry and climate (Carpenter et al., 2013; Saiz-Lopez et al., 2014). The reaction of iodide and ozone is not only a sink for ozone (Ganzeveld et al., 2009) but also a source of molecular iodine (I_2) and hypoiodous acid (HOI) to the atmosphere. These reactive iodine species photolyse to the highly reactive IO radical, influencing ozone cycling and other atmospheric chemistry reactions (e.g., Carpenter et al., 2013; Mahajan et al., 2010; Sherwen, Schmidt, et al., 2016). The iodine-driven

sea surface ozone sink has been identified as the most uncertain part of the tropospheric sink of ozone (Hardacre et al., 2015) and has been estimated to account for around 12% of the total (Sherwen, Evans, et al., 2016), and thus an understanding of ocean iodine cycling, and indeed global iodine biogeochemistry, is a key prerequisite for adequate models of ozone and atmospheric oxidation processes. We focus on inorganic iodine forms, as the interconversion of these is the predominant feature of the marine iodine cycle (e.g., Chance et al., 2014) and because the reaction of ozone and iodide accounts for around 75% of the sea-to-air iodine flux (Sherwen, Evans, et al., 2016). Volatile organic iodine compounds (VOI) such as methyl iodide, which are formed in the upper ocean by photodegradation of organic matter and direct production by phytoplankton (Stammler et al., 2013), make up the remainder of the sea-to-air iodine flux. However, VOI concentrations are typically several orders of magnitude lower than inorganic iodine concentrations, and they form a small component of the marine iodine cycle and will not be considered further in this study. We note that VOI production pathways may however be influenced by inorganic iodine cycling (e.g., Moore & Zafiriou, 1994)

Iodine is primarily present in the oceans as the dissolved inorganic ions iodide (I^-) and iodate (IO_3^-). In coastal surface water, an additional organic iodine form has been identified as a significant component of the iodine pool, although this is not seen in the open ocean (Luther et al., 1991). Iodine is known to be cycled biologically within the oceans leading to slight surface depletion of total iodine concentrations ($I^- + IO_3^-$) and a marked interconversion of iodine oxidation species with a euphotic zone maxima in iodide relative to iodate. In deep oxygenated waters, iodate is the overwhelmingly dominant species as predicted from its thermodynamic stability (Chance et al., 2014; Elderfield & Truesdale, 1980; Wong, 1991). The uptake of iodate and iodide and the release of iodide have been demonstrated in microalgal (e.g., Chance et al., 2007; de la Cuesta & Manley, 2009). In coastal surface water, an additional organic iodine form has been identified as a significant component of the iodine pool, although this is not seen in the open ocean (Luther et al., 1991). Surface water iodine speciation varies seasonally, with iodate decreases and iodide increases approximately in phase with cycles of primary production, although possibly with a time lag associated with delays between the uptake of iodate and its subsequent rerelease as iodide (e.g., Chance et al., 2010). Oxidation of this iodide back to iodate is estimated to have a timescale of the order of months to years, although it has not been measured directly because it is so slow (Campos et al., 1996; Chance et al., 2010; de la Cuesta & Manley, 2009; Edwards & Truesdale, 1997; Tsunogai, 1971; Waite et al., 2006). Several authors have noted a relationship between iodide and nitrate concentrations in surface water and speculated that this may reflect a real biogeochemical coupling of these species, which could reflect the geochemical similarities of iodate and nitrate. The evidence for such coupling has until recently been equivocal at best (Campos et al., 1999; Hung et al., 2005; Truesdale et al., 2000; Waite & Truesdale, 2003). Zic et al. (2013) and Truesdale et al. (2001) have demonstrated a link between the oxidation of ammonium to nitrite, and iodide to iodate, which has significant implications for our understanding of the ocean iodine cycle.

Although the global database for iodine speciation in ocean surface waters is rather limited, there are still clear large-scale patterns evident with iodide concentrations (and iodide/iodate ratios) much higher in the oligotrophic surface ocean gyre waters (>100 nM generally) than in high-latitude waters (<50 nM) (Chance et al., 2014), and this range of concentrations is sufficient to significantly affect the uptake of ozone and its global atmospheric cycling (Sherwen, Evans, et al., 2016). The realization of the importance of the role of iodine in surface ocean waters as a sink for ozone has led to efforts to incorporate this reaction into atmospheric models, which requires a global field of surface ocean iodide concentrations (Ganzeveld et al., 2009; Luhar et al., 2018). There have been some efforts to characterize the ocean surface iodide field in terms of other parameters that can be inferred indirectly or directly from satellite or other large-scale ocean databases, such as temperature and nitrate, and use the derived statistical relationships to predict the ocean surface iodide field, which can provide a boundary condition for atmospheric chemistry models (Sherwen, Evans, et al., 2016). The iodide distributions predicted by these statistical relationships basically reflect the large-scale ocean distribution of iodide with higher concentrations in low-latitude, high-temperature, low-nitrate waters and low-iodide concentrations at high latitudes in seasonally overturning cooler waters (Chance et al., 2014; MacDonald et al., 2014; Sherwen et al., 2019a). However, while the statistical relationships developed provide a generally good fit to the data, they are not based on the biogeochemical cycling of iodine in the oceans, and hence, their extrapolation beyond the data range for which the relationships are derived cannot be done with confidence, and hence, predictions of change in the

ocean iodide field with climate change, for example, are unreliable. It is also evident that iodide exhibits interannual variations (Chance et al., 2010), which may compromise these statistical methods.

We therefore present here the first ocean iodine biogeochemical cycling model that includes realistic phytoplankton uptake and release parameterizations of iodine cycling based on ocean primary production fields and iodide oxidation derived from laboratory-demonstrated mechanisms coupled to nitrogen cycling. This is all embedded within a realistic ocean physical mixing and transport field, allowing seasonal mixing between surface water where iodide is produced and subeuphotic zone waters, and redistribution by the local and global-scale circulation. We demonstrate that all of these biological and physical iodine cycling processes interact together to yield the observed global iodine distribution.

2. The Iodine Cycling Model

The iodine cycling model aims to capture the dominant biogeochemical processes involved in the cycling of iodine in the oxygenated ocean and embed these in a simplified three-dimensional circulation model of the upper ocean, driven by fields derived from climatologies and an ocean general circulation model. Further technical details and model equations can be found in Appendix A, and here, we summarize the key features of the model and its development.

2.1. The Physical Ocean Model

The model is global in coverage, with a horizontal resolution of 1° in latitude and longitude, and three layers in the vertical (Figure 1). The upper layer is the seasonal mixed layer, its thickness varying throughout the year (Monterey & Levitus, 1997). The middle layer extends from the base of the seasonal mixed layer to the maximum seasonal mixed layer depth (MLD), multiplied by 1.05, to prevent zero-layer thickness when the top layer is at maximum depth. The bottom layer has a thickness of 500 m, or extends to the ocean bottom (GEBCO—Becker et al., 2009) if this is less, or has a minimum depth of 0.05 times the maximum MLD if the mixed layer extends to the sea floor, to maintain a finite layer thickness. This simplification of the deep ocean structure reflects the constancy of iodine concentration and speciation at depth. Each layer is assumed to be completely mixed in the vertical. Changes in MLD result in the exchange of water and tracers between the upper two layers, and the exchanged tracers are mixed into the thickening layer. There is constant vertical mixing of 1×10^{-4} m^2 s^{-1} between the middle and bottom layers. Each vertical column is subject to a horizontal mixing of 2,000 m^2 s^{-1} and advection by the depth-dependent horizontal ocean currents derived from the OCCAM ocean GCM (see Aksenov et al., 2010, for details). Vertical advection is derived from the horizontal divergence of this flow, and the precipitation minus evaporation and runoff flux is accounted for at the surface.

2.2. The Biogeochemical Iodine Cycling Model

The iodine cycling model is embedded within this physical circulation model. Below the bottom model layer, it is assumed that the concentrations of iodide and iodate are 0 and 500 nM, respectively, broadly consistent with the observed global distributions in oxygenated waters (Chance et al., 2014).

Production of iodide only occurs in the mixed layer in the model and is assumed to be biologically mediated consistent with all the available evidence (Campos et al., 1996; Chance et al., 2007, 2010; Ducklow et al., 2018; Hepach et al., 2019; Tian et al., 1996; Wong, 2001). It is linked to the uptake of carbon by primary production via an iodine to carbon ratio, thought to be in the range 10^{-5} to 10^{-3} (Chance et al., 2010; Elderfield & Truesdale, 1980; Hepach et al., 2019; Jickells et al., 1988). Primary productivity is taken from the climatology of Behrenfeld and Falkowski (1997), which uses satellite observations to determine chlorophyll concentrations, and hence has no data where and when solar irradiance is low or zero. We could simply assume productivity is zero under these conditions, and this is supported at most longitudes where productivity is essentially zero at the poleward extent of the data, but in the North Atlantic in spring, the bloom extends to the northern limit of the data. We therefore extrapolate the productivity polewards from the last available data point to zero over 10° of latitude. We also assume no productivity under sea ice through multiplying the productivity by (1 − sea ice concentration) (Stroeve & Meier, 2018). It should be noted that for most longitudes and seasons, this results in the extrapolated productivity being zero in these regions beyond the data, so the correction is small.

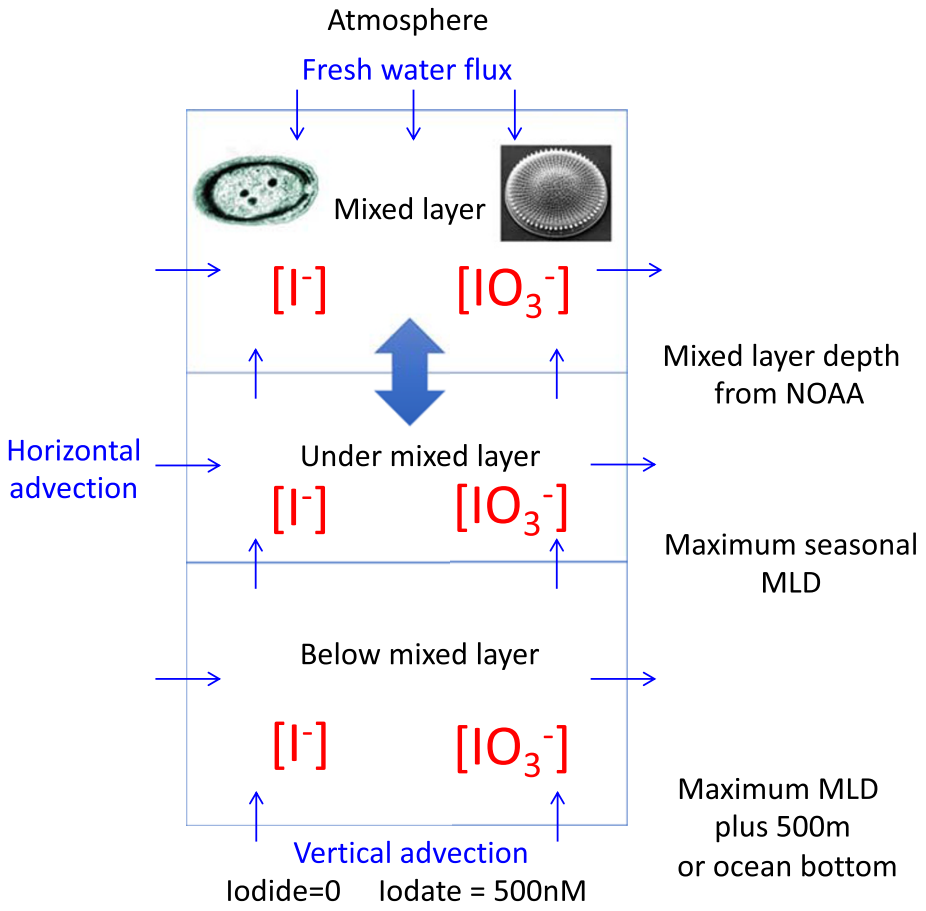

Figure 1. Schematic representation of the three-layer ocean model, in which the iodine cycling model is implemented. The upper layer is the mixed layer. The middle layer extends below this to the depth of the seasonal maximum mixed layer depth (multiplied by 1.05 to avoid zero depth in the model). The bottom layer extends either to the ocean floor or to a thickness of 500 m, whichever is less (but also has a minimum thickness of 0.05 times the maximum mixed layer depth to avoid zero thickness). Below the bottom box, iodide and iodate are assumed to have concentrations of 0 and 500 nM, respectively. Each box is subject to mixing and advection, and there is a freshwater flux due to precipitation, evaporation, and runoff through the surface of the upper box. See text for more details.

The phytoplankton-mediated conversion of iodate to iodide is assumed to occur during the senescence phase and is lagged 60 days from primary production (Bluhm et al., 2010; Chance et al., 2007, 2010; Hepach et al., 2019). It is assumed that the appearance of iodide in the water column occurs in tandem with the removal of iodate (as would be the case for a dissimilatory reduction mechanism) and hence that the particulate iodine reservoir in biomass is negligible. This is consistent with the near conservative behavior of total inorganic iodine seen in the upper ocean, where variations of 25% in speciation are accompanied by changes of only a few percent in total iodine (Truesdale et al., 2000). The widely reported inverse relationship between iodide and iodate also supports our assumption that iodate removal from the water column and iodide formation/release are directly coupled. It is found that the long-term equilibrium iodide concentrations are not sensitive to this lag timescale changing in the range 0–120 days (see section 4.3).

The rate of iodide production at low iodate concentrations is limited with an e-folding scale of 50 nM, to ensure that conversion from iodate to iodide tends to zero as iodate is depleted, but this only has a significant impact when iodate concentrations are less than around 100 nM, which is very rarely encountered in the model or observations. It should also be noted that any dependency of iodate to iodide reduction on iodate at higher iodate concentrations is not explicitly included in the model, because the I:C ratio is held constant regardless of the modeled ambient iodate concentration. With the exception of rare locations with unusually low iodate concentrations, the model implicitly assumes that the rates of both iodate reduction and bacterial iodide oxidation are biologically determined and are independent of substrate concentration.

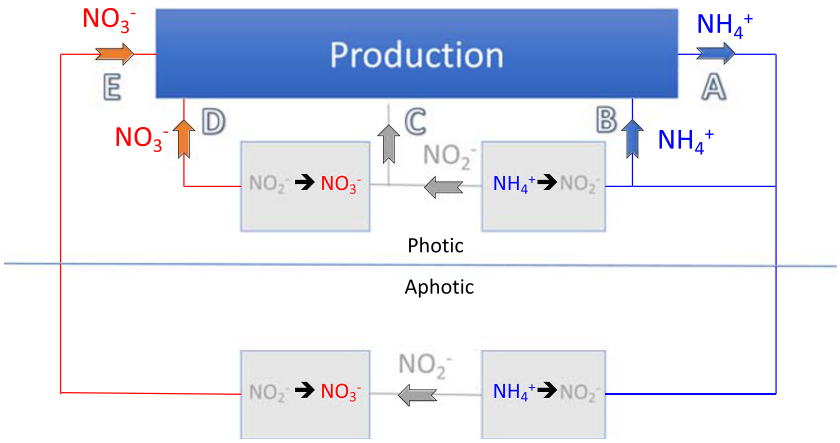

Figure 2. Schematic of nitrogen cycling in the ocean. Production is driven by nitrate (NO_3^-) originating from below the mixed layer, nitrate from nitrification within the mixed layer, and also ammonium (NH_4^+). Uptake of nitrite (NO_2^-) is much less and assumed to be zero. The proportion of nitrate supplied from below and within the mixed layer has been determined by Yool et al. (2007), allowing $D/(D + E)$ to be calculated, and hence the proportion of ammonium that undergoes oxidation to nitrite. It is this flux that is also associated with oxidation of iodide to iodate.

The processes governing the oxidation of iodide to iodate have not been well understood, but it is clear that the oxidation is slow with estimates varying from months to decades (Campos et al., 1996, 1999; Edwards & Truesdale, 1997; Jickells et al., 1988; Luther et al., 1995; Truesdale et al., 2000; Tsunogai, 1971; Waite & Truesdale, 2003), allowing time for physical water transport processes to play an important role in the iodide distribution. This uncertainty in oxidation rate estimates is at least, in part, due to a lack of knowledge as to whether or not the oxidation is biologically mediated. Truesdale et al.'s (2001) study in the Black Sea pointed to a possible role for nitrifying bacteria, and Long et al. (2015) found that iodide oxidation varied proportionally with nitrification in the South China Sea. Mixed layer nitrification results in the oxidation of ammonium, produced by the senescence of cells, to nitrite, and then nitrate (Figure 2), with the former transformation being linked to the oxidation of iodide. However, this is not the only route for ammonium loss in the euphotic zone, since it is also taken up by primary production and is subject to physical mixing and advection by the ocean circulation. The uptake of nitrite is thought to be negligible, and nitrate from mixed layer nitrification is available, together with "new" nitrate derived from upwelling, for driving primary production. A biogeochemical model including the process of mixed layer nitrification has been developed by Yool et al. (2007), resolved globally at a resolution of 1° latitude and longitude, and we have used this approach to allow us to separate the nitrogen cycle into the deep ocean nitrification route, and the mixed layer nitrification route, resolved globally at a resolution of 1° latitude and longitude. The proportion of nitrate available for production that comes from regeneration in the mixed layer (Figure 2, flux "D") is shown in Figure 3 (from Yool et al., 2007).

Production of iodide is linked to carbon fixation by an iodine to carbon (I:C) ratio and hence, via the Redfield ratio, is also linked to nitrogen uptake. Linking oxidation of iodide to nitrification in turn requires a stoichiometric link to nitrogen and carbon. We achieve this by using the well-established Redfield ratio of C:N = 106:16 and I:C = 3×10^{-4} reflecting the range reported in the literature, giving I:N = 0.002 for the oxidation of iodide with respect to nitrogen during mixed layer nitrification, provided we assume that the I:C and C:N associated with primary production are the same for bacterial nitrification.

We will see below that iodide oxidation by this mechanism has a profound effect on the iodide concentrations, as it results in a spatially variable, rapid, partial oxidation of the iodide inventory, with the remainder being subject to removal by ocean mixing and advection, and much slower chemical oxidation to iodate, which occurs implicitly below the layers represented in the model. This may also provide an explanation for the huge range of oxidation timescales reported in the literature (Campos et al., 1996; Chance et al., 2010; de la Cuesta & Manley, 2009; Edwards & Truesdale, 1997; Waite et al., 2006), with long timescales associated with environments where nitrification is weak/absent and much shorter timescales where nitrification is active. While the recycling of iodine between the iodate and iodide forms is substantial, the net cycling of

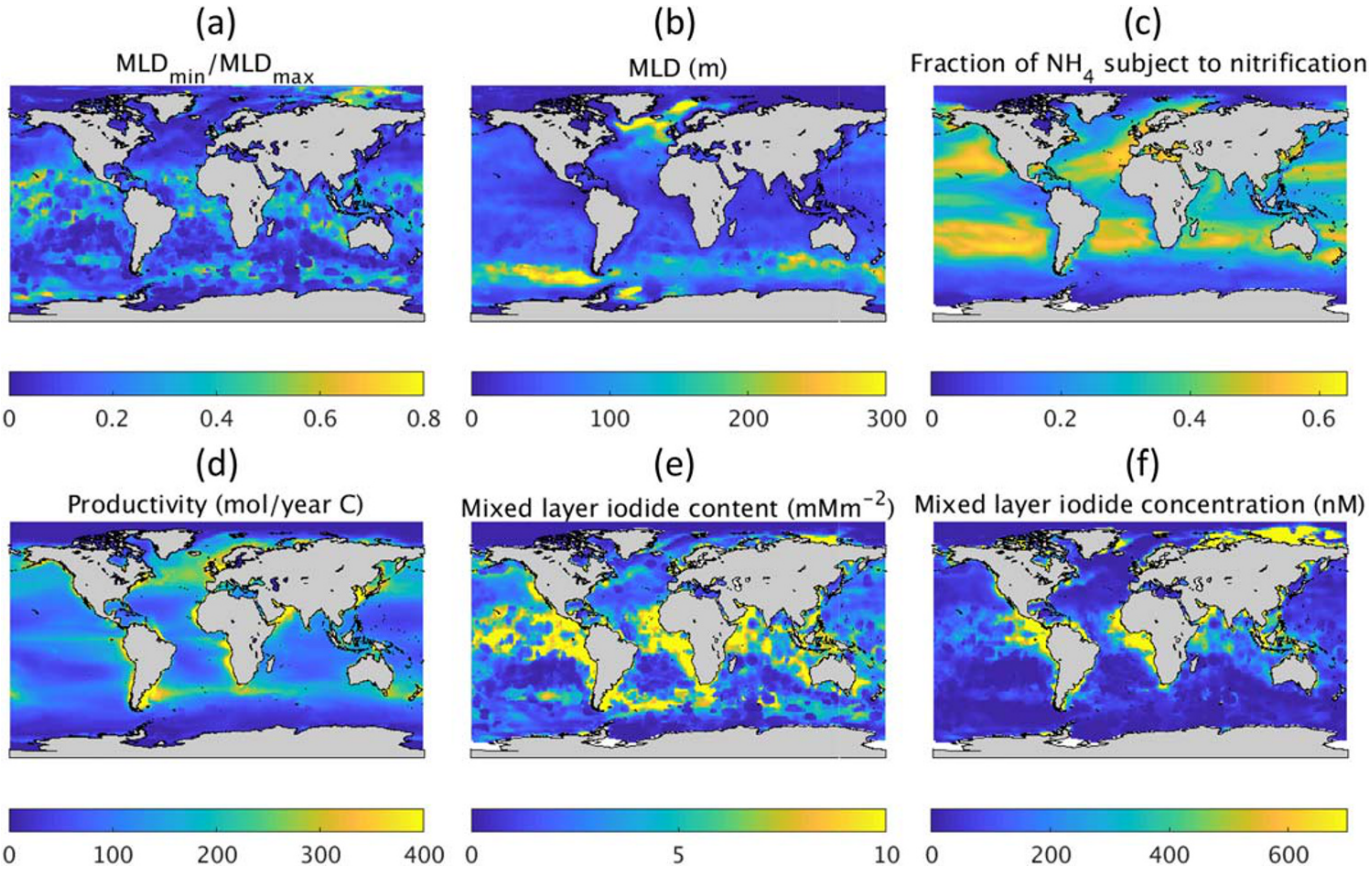

Figure 3. Parameters driving a simple model of oceanic iodide cycling and resultant iodide fields: (a) ratio of minimum to maximum mixed layer depth, (b) annual mean mixed layer depth, (c) proportion of ammonium subject to nitrification in the mixed layer (Yool et al., 2007), (d) ocean productivity (Behrenfeld & Falkowski, 1997), (e) predicted mixed layer iodide inventory, and (f) predicted mixed layer iodide concentration.

total iodine ($I^- + IO_3^-$) between the surface and deep ocean is small (there is generally <10% difference in total iodine concentration between surface and deep waters) and is ignored here, with total iodine treated as effectively conservative (Chance et al., 2014).

The deep ocean iodine cycle is represented in the model by the downwelling of iodide to the deep ocean, and the return of iodate to the bottom model level by upwelling, with a concentration of 500 nM. This assumes that iodide oxidation rates in the deep ocean are fast relative to deep ocean water residence times of decades to millenia and takes no account of low-oxygen environments where iodate reduction could occur, although these are of very limited extent in the present-day ocean.

2.3. Observed Iodide Concentrations

In any modeling study, observations are crucial to validate the model. Here, we have used iodide observations from the compilation described in Chance et al. (2019a), which is available from the British Oceanographic Data Centre (Chance et al., 2019b). This compilation includes almost all sea surface iodide observations reported in the literature, along with a number of unpublished data sets. The individual observations of iodide were then binned into a 1° latitude and longitude grid, for each of the three model levels, for each month of the year, and averaged where multiple observations occurred. Comparisons with the model were then made for the same month, in each location where observed iodide concentration data were present.

2.4. Modeling Strategy

In order to refine the iodine cycling model, we need to determine the I:C ratio and oxidation rate/mechanism that allows us to achieve the best spatial fit to the observed iodide distribution. Ideally,

we would like to find universal parameters that allow us to fit the data globally, in both coastal and open ocean locations, and are within the range reported in the literature. Iodide concentrations will be determined by a balance between production and loss, with production and weaker oxidation acting to increase the biogeochemical residence time (and vice versa), in conjunction with the residence time for water in the mixed layer, which is dependent on advection and mixing.

We will therefore run two suites of model experiments, one with the oxidation of iodide over a defined timescale and the other with oxidation linked to nitrification. In both of these, the I:C ratio will be varied over a range consistent with the values reported in the literature.

3. Results From a Simple Iodine Cycling Model

Before considering the results from the full iodine cycling model, we will consider a much simpler, conceptual box model, which will aid interpretation of the full model results.

The production and loss of iodide over an annual cycle can be captured by considering the dominant processes involved and assuming a vertical mixing timescale for iodide in the mixed layer of around 1 year. In the subtropical gyres, this timescale is likely to be considerably longer (e.g., Jickells et al., 1988), but elsewhere, it is plausible and provides a simple approach to investigate the dominant processes involved in determining iodide concentrations.

In this simple model, the annual production of iodide is assumed to be equal to the production of organic carbon, multiplied by an I:C ratio. Following an annual cycle of mixed layer deepening and shoaling, the proportion of iodide remaining in the mixed layer is assumed to equal MLD_{min}/MLD_{max}, with the remainder removed from the mixed layer during shoaling. The oxidation pathway driven by mixed layer nitrification converts a proportion of the iodide produced back to iodate. The residual iodide inventory is then distributed throughout the annual mean mixed layer to give a mean mixed layer concentration.

Figure 3 shows the components of this simple model. Productivity is high in regions where nutrients are supplied to the mixed layer by deep mixing, and in coastal regions, particularly where there is upwelling. This favors high iodide in these regions. Oxidation of iodide by nitrification is greatest in the subtropical gyres, lower in equatorial regions, and lowest at high latitudes, resulting from the link to the nitrification model of Yool et al. (2007). This results in the greatest oxidation of iodide in the subtropical gyres and lower latitudes outside of equatorial regions. MLD variations are generally greatest at high latitudes, resulting in the greatest loss of iodide through mixing, so long as the lifetime of iodide with respect to oxidation is comparable to the seasonal timescale of mixed layer cycling. The MLD itself is also greatest at high latitudes, although this has strong seasonal variability. These competing factors result in generally higher iodide concentrations at low latitudes, with the highest concentrations occurring where productivity is high, MLDs are shallow, seasonal MLD variations are small, and oxidation by nitrification is weak. In both the Atlantic and Pacific, this is on the eastern side of the basin, where predicted iodide concentrations are greatest. High iodide is also predicted in the Arctic, where productivity is lower, but MLDs are shallow and have little seasonal variation. The subtropical gyres have low iodide, due to low productivity and strong oxidation of iodide linked to mixed layer nitrification. The full model (section 4) will show that the iodide residence time is considerably longer than a year in these gyres, resulting in an underestimate by this simple model.

4. The Full Iodine Cycling Model

The model was run for a range of I:C ratios, from 4.7×10^{-6} to 1.2×10^{-3}, increasing in multiples of two. This range of values covers that reported in the literature (Chance et al., 2010; Elderfield & Truesdale, 1980; Hepach et al., 2019; Jickells et al., 1988). Two methods of iodide oxidation were used, first, a simple parameterization representing the actual processes by a timescale for conversion of iodide to iodate, and second, via a coupling to the nitrogen cycle through nitrification.

4.1. Oxidation Parameterized by a Timescale Conversion of Iodide to Iodate

The model was run with oxidation timescales of 1, 2, 4, 8, and 16 years, reflecting the large range of rates estimated in the literature (e.g., Campos et al., 1996; Edwards & Truesdale, 1997). Equation A.2.4a describes the process.

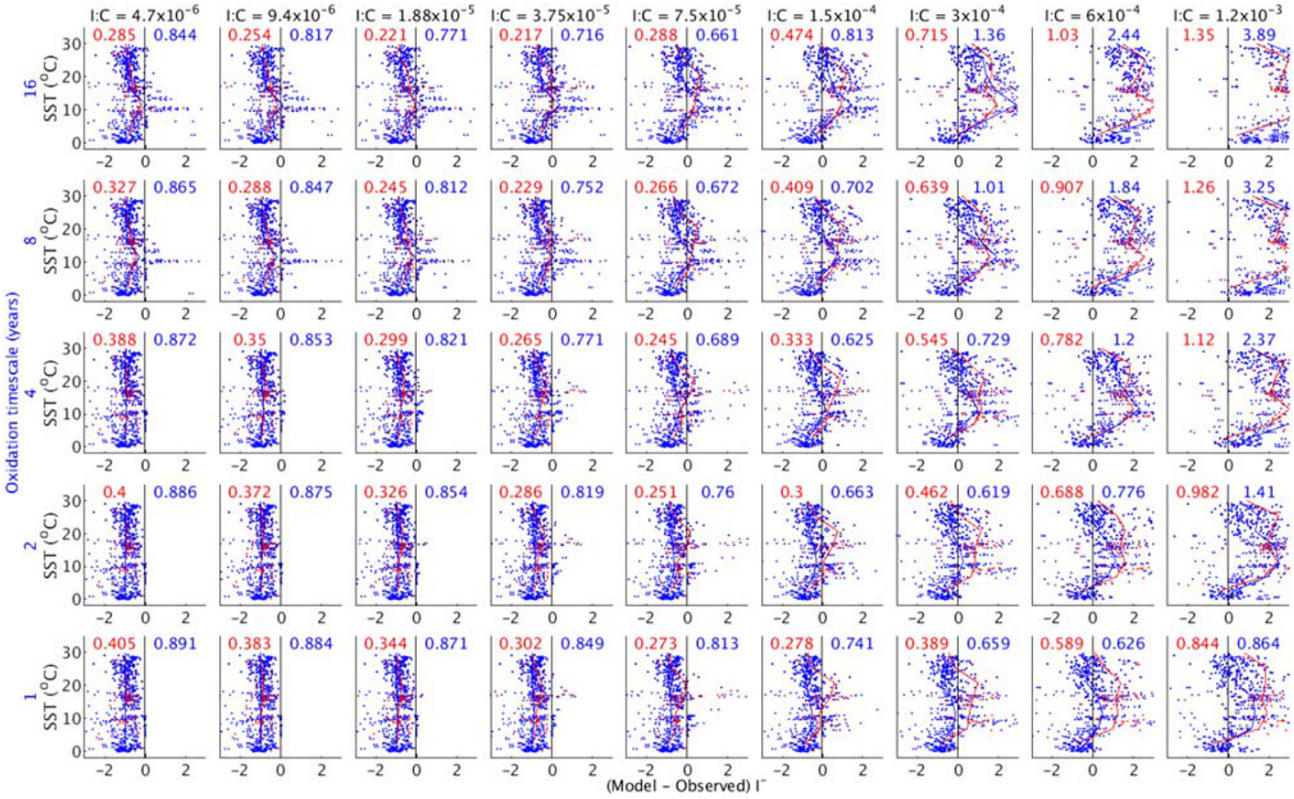

Figure 4. Normalized difference between modeled and observed iodide concentrations, as a function of SST, for a range of I:C production ratios, and iodide oxidation timescales. The RMS errors for coastal (<200 m) and open ocean (>200 m) locations are shown in red and blue, respectively.

For each model grid point where observations were available, the difference between the model and observed mixed layer iodine concentration was plotted as a function of SST (Figure 4) and hence broadly latitude. Increasing the I:C ratio increases production of iodide, and decreasing the oxidation timescale increases the rate of conversion back to iodate. Hence, with a low I:C ratio and long oxidation timescale, the predicted concentrations are generally higher than observed, whereas with a small I:C ratio, and short oxidation timescale, the model underestimates iodide concentrations relative to observed values.

At low SSTs (<5°C), agreement between model and observations is only achieved with higher I:C ratios, with the oxidation timescale having little influence. This is because there is a strong seasonal cycle in MLD, which acts to remove iodide from the mixed layer within an annual timescale and is the dominating iodide loss process.

For SSTs from 5°C to 15°C, model/observation differences can be minimized with appropriate I:C ratios and oxidation rates. At higher I:C ratios, the predicted iodide concentrations in coastal locations tend to be overestimated in comparison with open ocean locations, whereas with lower I:C ratios and longer oxidation timescales, both coastal and deep ocean locations are well represented by the model. The best fits lie in the parameter space between I:C $= 7.5 \times 10^{-5}$ with an oxidation timescale of 16 years and an I:C $= 6 \times 10^{-4}$ with an oxidation timescale of 1 year.

Above 15°C, the model/observation fit is more problematic. There is a consistent tendency across the I:C and oxidation timescale parameter space for a relative overestimation of modeled iodide compared to the available data between 15°C and 25°C (in the subtropical gyres), compared with an underestimation above these temperatures (in equatorial regions). This is the case in both coastal and open ocean locations. This could indicate that the I:C ratio is higher in equatorial regions than in the gyres or that oxidation is more rapid in the subtropical gyres. A variation in I:C ratio could be due to different types of plankton dominating primary production. An analysis of plankton type distributions (Alvain et al., 2008) does indeed show a separation of types between these regions, with *Synechococcus* dominating in equatorial regions, whereas

Prochlorococcus dominates in the subtropical gyres. The difference between model and observed iodide is consistent with work by Wong et al. (2002), who found that *Synechococcus* have some of the highest rates of iodide production.

A sensitivity experiment was performed, in which the rate of production of iodide from iodate was temperature dependent, increasing by twofold, fourfold, eightfold, and sixteenfold for a doubling of SST. It was found that an eightfold increase in production of iodide for a doubling in SST was required to remove the equatorial low-iodide bias, which is a far greater temperature dependency than permitted by physical chemistry alone (Luther et al., 1995). We therefore conclude that this is unlikely to be the reason for the model bias.

The dependence of iodide production on productivity is well established, but it is also noted that the model iodide biases are consistent with this dependency, with overprediction in midlatitude coastal regions and an underprediction in the low latitudes. A sensitivity experiment was performed in which the observed productivity was replaced with its globally averaged seasonal cycle. Interestingly, this considerably reduced the model biases, and we will see in section 4.2 that this is consistent with a link between production and oxidation, via the process of nitrification.

Another possible explanation for the poor fit of the model in some regions lies with the oxidation rate, which may vary spatially in the ocean. The representation of oxidation by a timescale is a simple approach designed to avoid use of a mechanism-dependent parameterization, be it physical chemistry (and therefore temperature dependent) or biologically mediated, which may also be temperature dependent. It should be noted that removal by mixing occurs in parallel to these processes and is represented by the model. With the exception of processes in the sea surface microlayer, the purely chemical oxidation of iodide in the seawater is thought to be so slow that it can be considered insignificant (Luther et al., 1995). This rate would increase with temperature and therefore result in a greater oxidation of iodide in equatorial regions, where the model is underestimating concentrations. Inclusion of a temperature-dependent oxidation rate would therefore increase the tendency for the model to underestimate concentrations in equatorial regions.

4.2. Oxidation Driven by Mixed Layer Nitrification

Biologically mediated iodide oxidation by bacteria has been shown to occur (Amachi et al., 2004, 2005; Fuse et al., 2003; Gozlan, 1968), and recent studies have demonstrated that it may be brought about by nitrifying bacteria (Truesdale et al., 2001; Zic et al., 2013). This discovery prompted the inclusion of nitrification-linked oxidation in the model.

This mechanism is discussed in section 2.2 and is described by Equation A.2.4b. The linking of the oxidation of iodide to nitrification, at a ratio stochiometrically consistent with that of iodide production, results in a proportion of the iodide produced being oxidized to iodate over a timescale of days, assuming iodide is released during senescence and ammonium oxidation has a timescale of days (Yool et al., 2007), while the remainder is subject to oxidation by an unspecified, possibly purely chemical process (which we will assume has a much longer timescale) and physical mixing. Figure 3 (top-right) shows the proportion of mixed layer nitrate supplied by nitrification, corresponding to the proportion of iodide subject to oxidation, as calculated by Yool et al. (2007). It is immediately apparent that the largest proportion of iodide subject to oxidation is in the subtropical gyres, where the model overestimates iodide concentrations.

The model was run with the same range of I:C ratios, but with this alternative oxidation mechanism. The general response to changing I:C ratio is the same as with oxidation over a prescribed timescale (Figure 5), but the overestimation of iodide for SSTs in the range 15–25°C is considerably reduced, for both coastal and open ocean locations, with the best fit obtained using an I:C ratio of 3.75×10^{-5} similar but about 2 times lower than in previous model runs. This value is within the range reported in the literature and corresponds well to the ratio found for some types of phytoplankton (Hepach et al., 2019) and in oceanic studies (Campos et al., 1996; Chance et al., 2010).

Linking oxidation to nitrification fundamentally changes the way iodine is cycled between iodate and iodide. Previous assertions that oxidation occurred at a given rate, which is possibly temperature dependent, and/or biologically mediated, and hence spatially variable, fail to capture a key aspect of the process that results from the link to nitrification. The oxidation of iodide back to iodate in tandem with the oxidation of ammonium results in a proportion of the iodide being oxidized rapidly in the surface layer (timescale order days, Yool et al., 2007), while the remainder is removed from the mixed layer by a slower physical mixing pathway

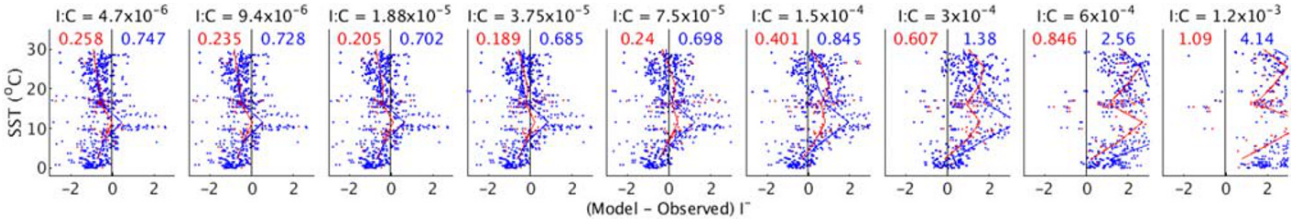

Figure 5. Normalized difference between modeled and observed iodide concentrations, as a function of SST, for a range of I:C production ratios, with iodide oxidation driven by nitrification. The RMS errors for coastal (<200 m) and open ocean (>200 m) locations are shown in red and blue, respectively.

to the ocean interior where much slower oxidation occurs. In regions where vertical mixing is strong (e.g., high latitudes), mixing is the dominant removal mechanism, and iodide has a residence time in the surface waters of around 1 year. However, where vertical mixing is much less intense (e.g., the subtropical gyres), the proportion of iodide remains unoxidized and therefore accumulates year on year and is slowly mixed out, resulting in a much longer residence time of the iodide in the surface waters. This coupling of iodide oxidation to the euphotic zone biogeochemistry of nitrogen may help explain why there is such a large range of oxidation timescales reported in the literature (Campos et al., 1996; Edwards & Truesdale, 1997; Tsunogai, 1971; Truesdale et al., 2001; Žic & Branica, 2006; Zic et al., 2013), as the actual removal process comprises rapid oxidation of part of the iodide inventory in conjunction with nitrification, and the relatively slow physical removal of the remainder by mixing to the ocean interior, followed by slow chemical oxidation.

4.3. Comparison With Observed Ocean Sections

We will now make comparisons between the modeled and observed iodides for five ocean sections: a transatlantic meridional section (Truesdale et al., 2000), a South Atlantic meridional section (Campos et al., 1999), a South Atlantic zonal/meridional section (Bluhm et al., 2011), an East Atlantic meridional section (data collected by Alex Baker et al.), and an Indian Ocean section (data collected by Rosie Chance/Liselotte Tinel et al.). All the data used for these comparisons are described in Chance et al. (2019a) and are available from the British Oceanographic Data Centre (Chance et al., 2019b). Model comparisons with ocean sections allow spatial and interbasin comparisons to be made.

We have seen in section 4.2 that while a best fit between model and observations can be made by selecting an appropriate I:C ratio, there is still considerable variation between the model and observations at each particular SST. Figure 6 shows comparisons between model and observed iodide concentrations for each section and for a range of I:C ratios. Taking each section in turn, it can be seen that the model can be made to fit each section with considerable skill but that a different I:C ratio is required for each section. The two meridional Atlantic sections (extending from 45°S to 45°N) require a relatively low ratio of 1.9×10^{-5}. The two South Atlantic sections require a higher I:C ratio, and it is apparent that within the latitudinal range of these sections, the best fit requires an increasing I:C ratio with increasing latitude. The Campos et al. (1999) section is in best agreement with the model with an I:C of 3×10^{-4} south of 50°S, increasing to 3.8×10^{-5} at 30°S. The Bluhm et al. (2011) section fits best with an I:C of 3×10^{-4} to 6×10^{-4} between 70°S and 60°S. The Indian Ocean section fits best with an I:C of 3×10^{-4} south of 20°S, but with a much lower value of around 1×10^{-5} near the equator. It is clear that the I:C ratio required to fit the model to the observations is around 10 times greater at high latitudes than low latitudes. However, it is also interesting to note that a relatively high ratio is required in the Indian Ocean south of only 20°S.

5. Discussion

Having established that the model is capable of reproducing the observed iodide distributions with an appropriate I:C ratio consistent with the relatively wide range of values reported in the literature, and an oxidation mechanism that has been shown to occur, we will now use the model to broaden our understanding of the role of processes in the ocean iodine cycle.

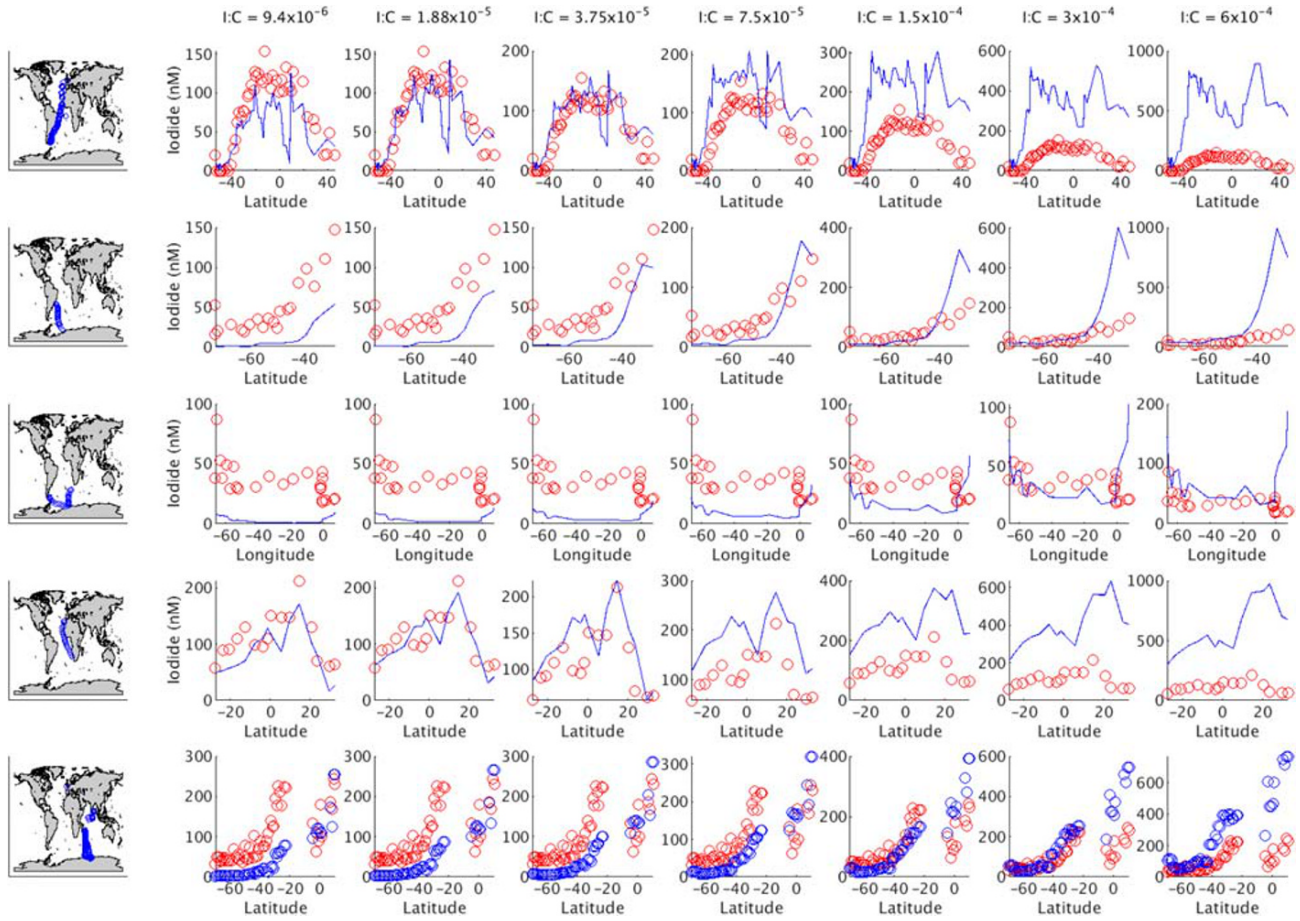

Figure 6. Comparison between modeled and observed iodide for a range of I:C production ratios, for five ocean transects—from top to bottom, Truesdale et al. (2000), Campos et al. (1999), and Bluhm et al. (2011), data collected by Alex Baker et al., and data collected by Rosie Chance/Liselotte Tinel et al., all taken from Chance et al. (2019a, 2019b).

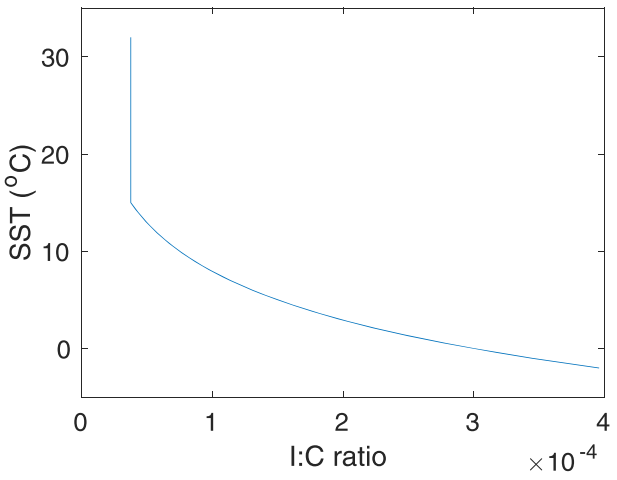

Figure 7. I:C production ratio that gives the best model—observation fit (lowest RMS error), as a function of SST.

5.1. Spatial Variation of the I:C Ratio

The finding that the I:C ratio varies spatially raises the question of whether a global field of I:C can be derived from the model. There is no reason to expect the I:C ratio to be globally constant; even the Redfield ratio of C:N:P has in reality some variability, and the variability for other elements may be greater (Moore et al., 2013). The RMS error between the model and iodide observations was calculated for each model I:C ratio, in bins of 5°C increments in SST. An empirical function describing the optimum I:C ratio required to minimize the model RMS error is shown in Figure 7. The optimum I:C ratio decreases with increasing SST from 3×10^{-4} at 0°C to 3.8×10^{-5} at SSTs of >15°C. The spatial distribution of I:C derived from this function is shown in Figure 8a.

An alternative approach is to derive a zonally constant I:C, taking the zonal mean of the best fit I:C ratio for each iodide observation point. We have already seen that the best fit I:C ratios in the Indian Ocean south of 20°S are greater than in the Atlantic, so we derive a separate zonal mean for the Indian Ocean from the Atlantic and poorly observed Pacific oceans, with a smooth transition between the

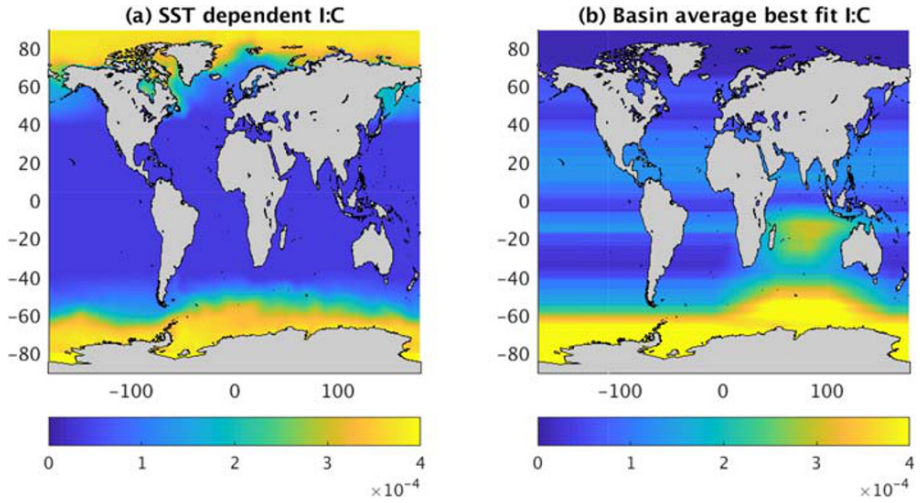

Figure 8. I:C production ratio derived from (a) a best fit to SST, using the relationship in Figure 7 and (b) using the zonal mean of the best fit I:C for the Atlantic and Pacific, and Indian oceans.

ocean basins. It should be noted that in the absence of any observations in the Arctic, the I:C ratio was set to that at the latitude of the northernmost observation in the Atlantic. This I:C field is shown in Figure 8b. The SST-derived field has a much higher I:C ratio in the Arctic, which is a result of the observational evidence from the Southern Ocean with similar SSTs. The zonal mean approach results in more latitudinal structure in the I:C ratio, including a marked asymmetry in the subtropical Atlantic, and a much greater I:C in the subtropical Indian Ocean.

Figure 9 shows the comparison between the model and observations for each of the five ocean sections, for constant, SST-dependent and zonal basin mean I:C fields. The use of a globally constant I:C ratio results in a generally poor fit, with the model underestimating iodide at high latitudes and in the Indian Ocean south of 20°S. The high-latitude fit can be improved by using a greater I:C ratio, but low-latitude iodide is then overestimated. The SST-dependent I:C ratio performs more consistently across the sections, with only the midlatitude Indian Ocean showing significant discrepancies. The use of a zonal basin average I:C results in a much better fit in the Indian Ocean, where I:C is increased, but the model overestimates iodide in the low and midlatitude Atlantic. The location of the iodide observations in the Atlantic tends to coincide with anomalously low SST for the latitude, so longitudinal extrapolation of the I:C ratio favors a higher I:C ratio than the SST-derived ratio, due to the inverse relationship between I:C and SST/latitude.

Overall, the modeled iodide is in best agreement with observations when the I:C ratio is parameterized as a function of SST, as shown by the RMS errors (Figure 10). The model still tends to underestimate iodide where SST > 20°C and overestimate for 5°C < SST < 15°C. It might be expected that the dependency of the I:C ratio on SST would eliminate this bias completely, but the residual differences between the model and observations are consistent with the ocean circulation playing an important role in redistributing iodide across SST contours. Selection of the best fit I:C ratio assumed that the iodide depended only on the local I:C ratio, whereas advection could potentially bring iodide from lower-latitude regions where the best fit I:C is lower and higher-latitude regions where the best fit I:C is greater. Since the I:C ratio was globally constant in the suite of model runs from which the local best fits were determined, the I:C ratio and iodide concentrations at lower latitudes would be too great and at higher latitudes too small with respect to the SST-dependent I:C ratio case. Thus, in the runs used to determine the best fit I:C ratio, advection of iodide from regions with higher SST and I:C ratio is too great and from lower SST and I:C ratio too small. This is consistent with the tendency of the model to underestimate iodide at low latitudes and overestimate at mid-latitudes. This suggests that the surface water iodide residence time is sufficiently long that horizontal as well as vertical mixing processes may be important. We also suggest that the I:C ratio may vary systematically with SST, which probably implies a variation with phytoplankton species and communities.

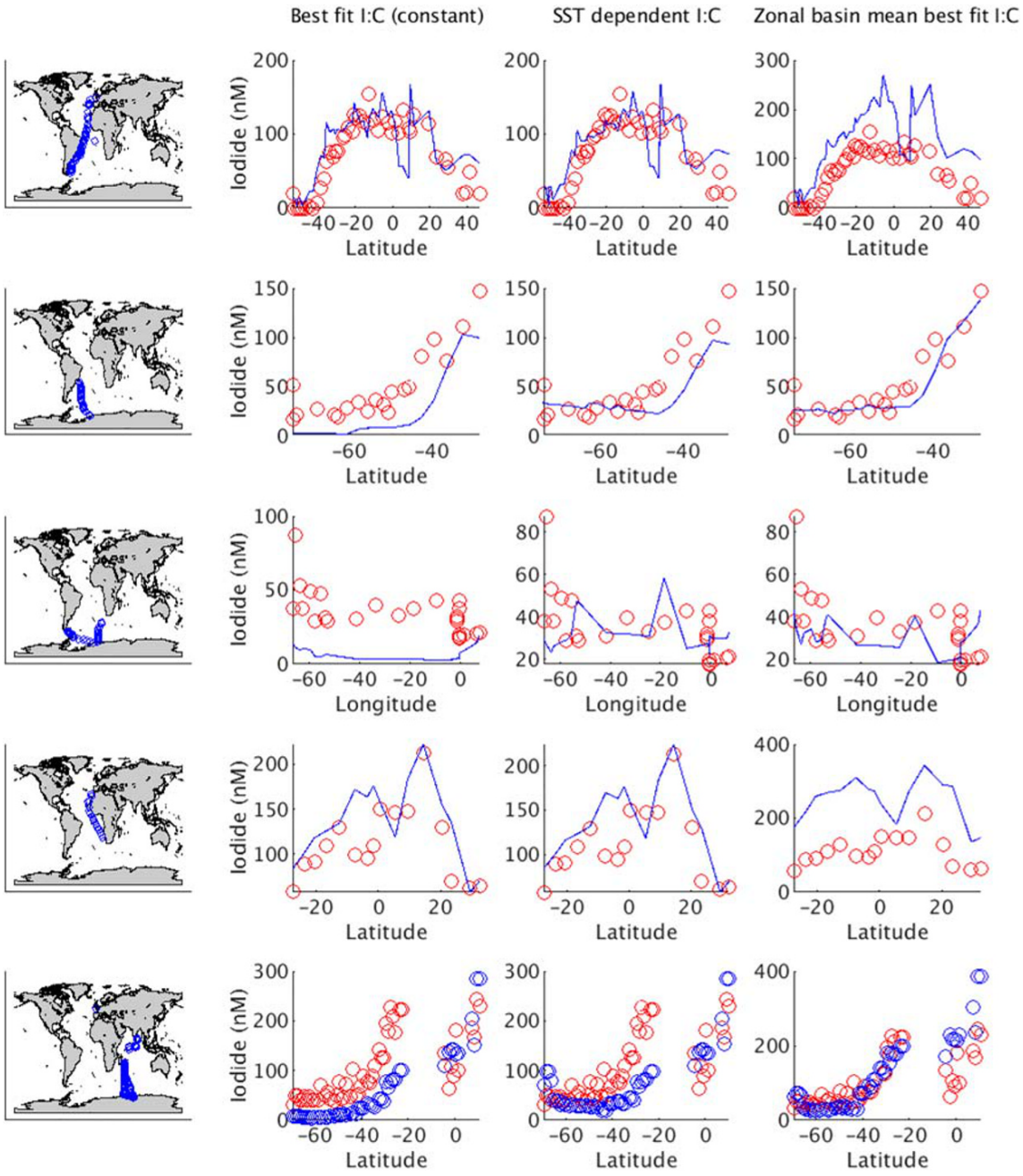

Figure 9. Comparison between modeled (blue) and observed (red) iodide for five ocean transects—from top to bottom, Truesdale et al. (2000), Campos et al. (1999), and Bluhm et al. (2011), data collected by Alex Baker et al., and data collected by Rosie Chance/Liselotte Tinel et al., all taken from Chance et al. (2019a, 2019b). The first column shows results for the best fit globally constant I:C production ratio, the second for an SST-dependent I:C production ratio (see Figure 8a), and the last a zonal mean I:C production ratio for the Atlantic and Pacific, and Indian oceans.

5.2. Comparisons With Statistically Derived Surface Iodide Fields

Modeling the ocean iodine cycle has produced a new estimate of surface iodide concentrations, which can be compared with other estimates from existing statistical and nonparametric machine learning methods. These statistical methods attempt to fit the observed iodide data using a suite of correlations to other more widely observed ocean variables including temperature, salinity, MLD, and nitrate. Here, we will use the model configuration that uses an SST-dependent I:C ratio, as this has a lower RMS error with observations than the latitude/basin I:C-dependent approach. Comparing the model iodide field with observations, where

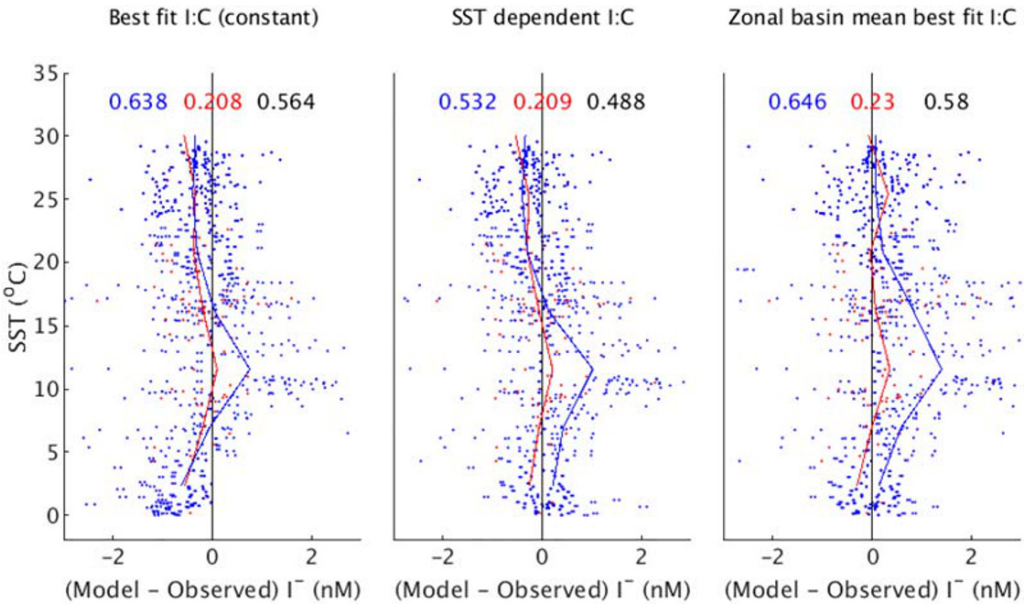

Figure 10. Normalized difference between modeled and observed iodide concentrations, as a function of SST, for a range of I:C production ratios, and iodide oxidation timescales. Left: for the best fit globally constant I:C production ratio, middle: for an SST-dependent I:C production ratio (see Figure 8a), and right: a zonal mean I:C production ratio for the Atlantic and Pacific, and Indian oceans (see Figure 8b). The RMS errors for open ocean (>200 m), coastal (<200 m), and all locations are shown in blue, red, and black, respectively.

they exist, shows a generally good agreement between the model and observed values (Figures 11a–11c), with the model tending to slightly overestimate iodide in the Atlantic and underestimate iodide in the Indian Oceans, as we have seen in previous sections. Elevated concentrations are generally confined to the eastern and coastal regions of the low-latitude and midlatitude ocean basins, and it is interesting to note that the majority of the observations are in these regions. High iodide is also predicted in the Arctic, but no direct observations are available to support this. However, periods of low tropospheric ozone in the atmospheric boundary layer during spring, driven from the ocean surface, have been observed in the Arctic (Wessel et al., 1998). This depletion of tropospheric ozone could be driven by iodine emissions from the Arctic Ocean.

Chance et al. (2014) proposed a parameterization of iodide in terms of a number of oceanic variables (Figure 11d). This has a strong dependency on latitude but does not predict much variation with longitude. Where observations exist, agreement with iodide concentrations predicted by the model and those predicted by the Chance et al. (2014) equation is good, but elsewhere, large differences exist (Figure 11e).

MacDonald et al. (2014) also parameterized iodide concentrations, but used a simpler approach, relating $\ln(I^-)$ with SST^{-1} using a subset of the observational database in Chance et al. (2014) (Figure 11f). This parameterization is currently the most widely used in atmospheric models (e.g., Sarwar et al., 2016; Sherwen, Evans, et al., 2016). Iodide fields predicted using this relationship are again broadly consistent with observations where they exist but are lower than the Chance et al. parameterization over much of the low latitudes and midlatitudes, away from the regions with observations. The MacDonald parameterization generally predicts lower iodide concentrations than the model at high latitudes and higher concentrations at low latitudes (Figure 11g). This pattern is consistent with using just SST as a predictor of iodide, compared to the model approach that incorporates a range of processes.

Sherwen et al. (2019a) adopted a machine learning approach to predict iodide from an expanded compilation of iodide observations (Chance et al., 2019a, 2019b). This approach assigns an iodide concentration to each oceanic location based on observed iodide values at locations with related combinations of biogeochemical and oceanographic properties. This machine learning-based parameterization yields a similar iodide distribution to that predicted by the multivariate equation in Chance et al., but with generally greater iodide at

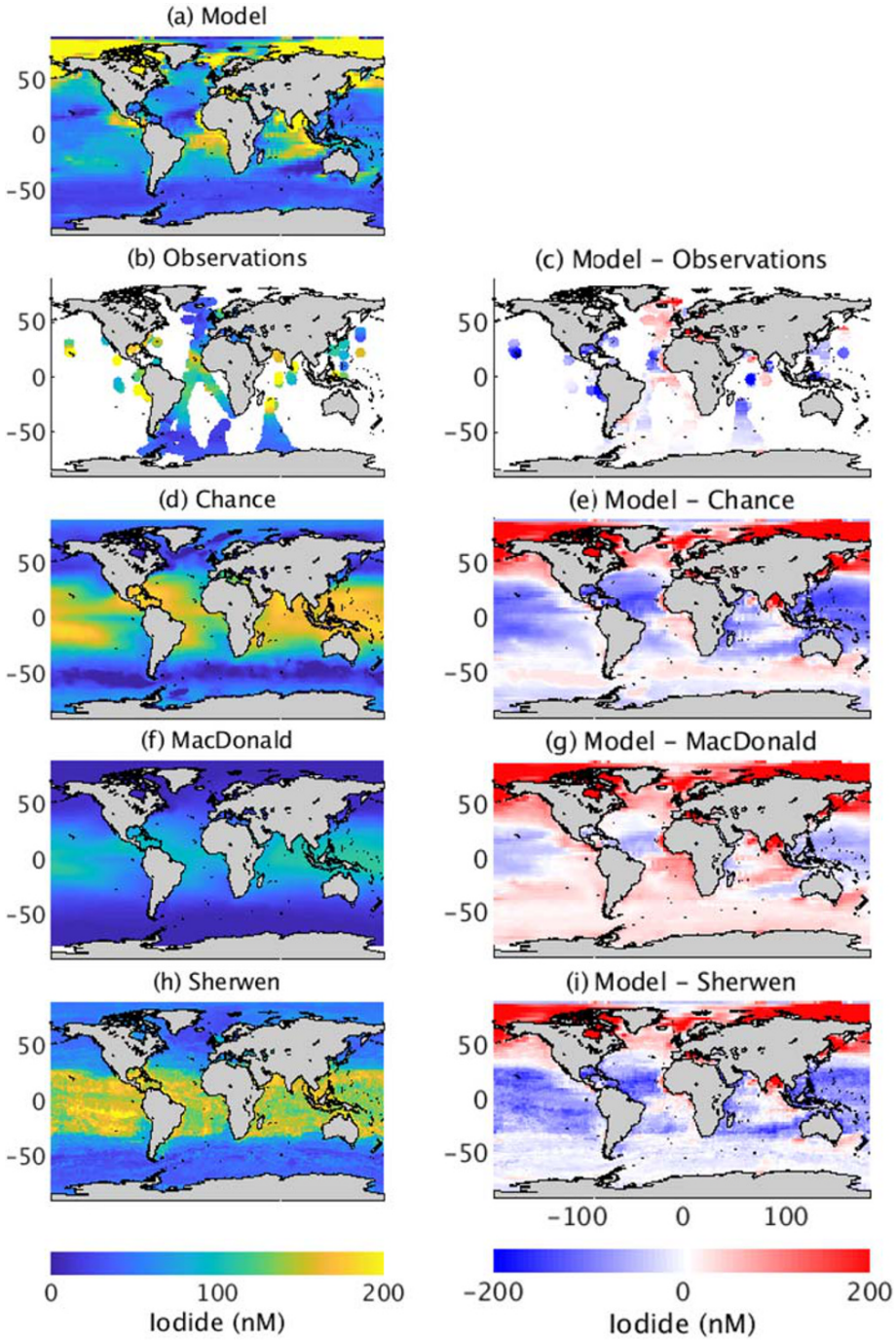

Figure 11. Comparison of model-predicted annual average mixed layer iodide concentration with observations and other predictions. From top to bottom: (a) from the model, using an SST-dependent I:C production ratio, (b, c) from observations (Chance et al., 2019a, 2019b), (d, e) from the parameterization of Chance et al. (2014), (f, g) from the parameterization of MacDonald et al. (2014), and (h, i) from the machine learning parameterization of Sherwen et al. (2019a, 2019b). Differences with the model are shown in the right-hand column.

higher latitudes (Figure 11h). This is consistent with both methods using similar oceanic properties (e.g., SST, salinity, and nitrate) to predict iodide. Comparison of model and machine learning predictions shows that the latter technique predicts higher iodide throughout most of the ocean (Figure 11i).

In each comparison, the modeled iodide has more longitudinal variation than the statistical methods suggest. Observations are currently insufficient to assess whether such a longitudinal variation does in fact

exist. Observations of iodide have mostly been concentrated around the periphery of ocean basins, leaving most of the subtropical gyres poorly sampled. It is in these regions that the Chance et al. (2014) and Sherwen et al. (2019a) parameterizations predict relatively high-iodide concentrations, consistent with the observations at similar latitudes, whereas the model predicts lower iodide, predominantly as a result of taking into account lower productivity and increased nitrification-dependent oxidation in these regions. Meanwhile, the model predicts higher iodide concentrations in the Arctic than the other approaches. This is because, within the model, advection redistributes iodide within the ocean gyres and also supplies iodide to the Arctic. The interaction of these, and other processes, means that iodide cannot simply be described by local oceanic conditions but requires an ocean circulation model to support the biogeochemical transformations involved in the oceanic iodine cycle. Given this, we suggest that the modeled distribution of iodide is likely to give a more accurate estimate of the ocean surface iodide distribution than methods based on local relationships alone. Future observations of iodide in currently unsampled regions such as the Arctic and subtropical gyres will prove crucial in determining whether the modeled field is accurate.

5.3. The Role of Individual Processes in Determining Surface Iodide

Modeling of the ocean iodine cycle allows us to investigate which oceanic and/or biogeochemical processes are important in determining iodide concentrations. A suite of sensitivity experiments was performed to investigate this, using the I:C ratio dependent on SST (Figure 12). The production of iodide is dependent on productivity. The seasonal cycle of carbon and hence iodide production could impact iodide concentrations via the seasonal MLD cycle. A model run with the local seasonal cycle of production replaced by the annual mean resulted in small decreases in iodide in some coastal and subtropical regions, where seasonal maxima in production coincide with shallow MLDs, and an increase around Antarctica, where production precedes the MLD minima (Figure 12a). Halving the productivity reduces iodide, with the greatest reductions in subtropical regions where iodide concentrations are greatest (Figure 12b).

Removal of the seasonal cycle of MLD increases iodide over most of the ocean, consistent with the reduced loss from vertical mixing (Figure 12c). However, in the subtropical South Pacific, concentrations decrease. Examination of the iodate field shows increased mixed layer depletion of iodate widely across the subtropics, and in the Arctic, when MLD variations are removed, together with the supply of iodate from below the mixed layer. In the South Pacific subtropical gyre, this depletion is sufficient to limit iodide production. Doubling the MLD effectively doubles the volume of water in which the iodide is stored and therefore reduces iodide concentrations accordingly (Figure 12d). Iodide increases in some high-latitude locations, but this is because the MLD increase is limited by the ocean depth, so where the maximum MLD extends near to the ocean floor, the seasonal MLD variation is effectively reduced, reducing the seasonal loss each year.

Oxidation of iodide to iodate acts to reduce iodide concentrations, hence removing the oxidation process increases iodide, especially in the subtropical gyres. It is here that oxidation is the dominant removal process, as vertical mixing is weak. At high latitudes, where removal is dominated by the seasonal cycle of MLD, oxidation has a much smaller impact (Figure 12e).

Advection redistributes heat and salt, and also all other tracers, around the ocean. The impact of this advection depends on the lifetime of the tracers and their spatial gradients. Removal of advection from the model results in increased iodide everywhere except the Arctic (Figure 12f). This shows that the vertical component of the circulation acts either to reduce iodide through the upwelling of iodide-depleted water or to remove iodide through the downwelling of iodide-rich water, the net effect of both of which is to remove iodide to depth, where it undergoes long-term oxidation to iodate. In the Arctic, however, iodide decreases without advection, showing that at least part of the iodide results from advection from the North Atlantic, probably associated with the spring bloom. Truesdale et al. (2003) also found iodide concentrations to be dependent on advection in the Skagerrak.

Iodide is thought to be released from most types of phytoplankton cells during the senescence phase (Bluhm et al., 2010), with a lag estimated at around 60 days. The sensitivity of iodide concentrations to this lag was tested by using lags of 0 and 120 days in the model. Earlier release results in an increase in iodide in some coastal locations and in the Arabian Sea. Delayed release results in a small decrease in iodide in some

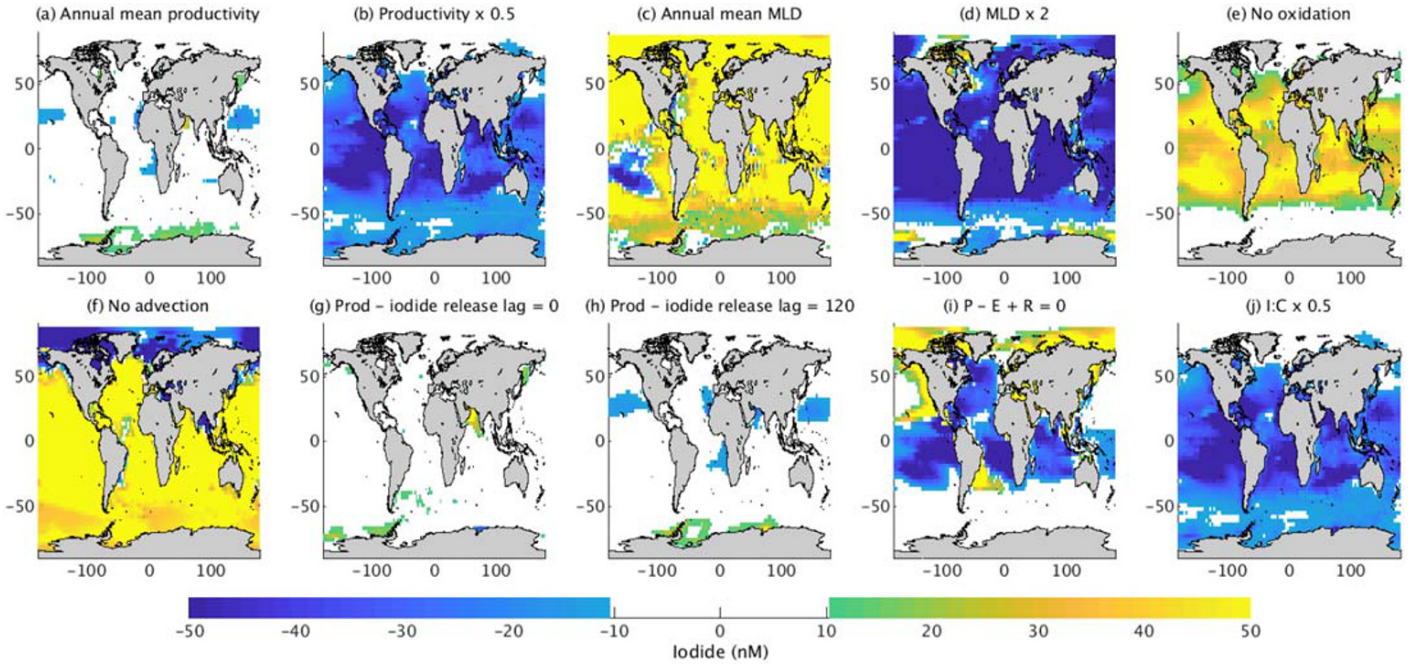

Figure 12. Sensitivity of the modeled mixed layer iodide concentration to forcings and processes in the model. Annual mean mixed layer iodide concentration difference between perturbed and control run for (a) production with seasonal cycle removed, (b) productivity halved, (c) seasonal mixed layer depth variations replaced by annual mean mixed layer depth, (d) mixed later depth doubled, (e) no oxidation of iodide, (f) no horizontal or vertical advection, (g) iodide release from cells at same time as carbon production, (h) iodide release from cells 120 days after carbon production (standard model lag is 60 days), (i) zero surface freshwater flux due to precipitation, evaporation, and runoff, and (j) I:C production ratio halved.

midlatitude locations (Figures 12g and 12h). These changes are due to the interaction of the release of iodide with seasonal MLD variations.

The net surface freshwater flux, resulting from precipitation, evaporation, and runoff, acts to dilute/concentrate the mixed layer. Removal of the freshwater flux has a corresponding impact on iodide concentrations. Net freshwater input dilutes iodide at high latitudes, whereas net freshwater loss concentrates iodide. This has a significant impact where MLDs are shallow, and the flux is large (Figure 12i), for example, the Arctic.

Lastly, the I:C ratio for the production of iodide acts as a multiplier to the production of C, and the impact of changes in the I:C ratio corresponds to changes in productivity (Figures 12j and 12b).

These model sensitivity tests give an important insight into the processes driving ocean iodide concentrations and show that surface iodide concentrations result from the interaction of several processes, which are dominated by primary productivity, the I:C ratio, MLD, oxidation, advection, and the oceanic freshwater flux. All of these are likely to change during the coming decades and centuries as atmospheric greenhouse gas concentrations increase, and impact climate and ocean chemistry. For instance, heating of the upper layers of the ocean may reduce MLDs, and nitrification rates may decrease due to ocean acidification (Beman et al., 2011), resulting in less oxidation. Both of these changes would act to increase iodide concentrations. Further studies would be needed to quantify potential future changes in the ocean iodide cycle.

6. Conclusions

We present the first physical and biogeochemical model for the cycling of iodine in the ocean. In the model, production of iodide from iodate is driven by primary production, and it is found that the I:C ratio for production of iodide increases by an order of magnitude between low and high latitudes, yet this range lies within those reported in the literature. Evidence from oceanic and laboratory-based studies shows a link between the oxidation of iodide and ammonium by nitrification. In the model, it is found that the spatial distribution of observed iodide can best be reproduced if oxidation is also linked to nitrification, which has a distinctive spatial pattern. Using the model to explore the sensitivity of surface iodide reveals that the distribution

results from several interacting processes, both physical and biogeochemical, and that changes in any of these are likely to result in changes to surface iodide concentrations. Significant differences are found between global surface iodide distributions derived from parameterizations and those predicted by the model. The model predicts much greater longitudinal variations of iodide within ocean basins, which cannot be captured statistically from the predominantly meridional observational transects. The model also predicts high-iodide concentrations in the Arctic, where there are currently no observations. These aspects of the iodide distribution are consistent with advection of iodide within the ocean gyres and major currents linking ocean basins, reflecting the relatively long lifetime of iodide in surface waters, which cannot be captured by statistical relationships between iodide and local oceanic variables. The cycling of iodine in the ocean is linked to the atmospheric cycling of iodine and ozone in a large-scale global biogeochemical cycle. The model-predicted surface iodide distribution differs sufficiently from that derived by statistical and machine learning techniques to impact atmospheric model predictions of ozone and air quality. We now await new observations of iodide in regions currently without observations (in particular the Arctic and centers of the subtropical gyres) to further validate our process-based prediction of surface iodide concentrations.

Appendix A: The Ocean Iodine Cycling Model

A.1 Model Description

The ocean iodine cycling model represents the interconversion of iodine between the two species iodate (IO_3^-) and iodide (I^-). The model is initialized with all the iodine in the form of iodate, with a concentration of 500 nM, corresponding to the global mean of the sum of iodide and iodate species (Chance et al., 2014). Conversion of iodate to iodide is driven by a global monthly climatology of primary production (Behrenfeld & Falkowski, 1997), at a rate linked to the rate of carbon assimilation multiplied by an iodine to carbon ratio, and lagged by 60 days from the associated primary production (Bluhm et al., 2010; Chance et al., 2010; Hepach et al., 2019). A saturation term is used to limit iodate to iodide conversion as iodate becomes depleted below 50 nM, although this low iodate concentration is rarely seen in the existing observations or model runs. Iodide production occurs only in the mixed layer (Equation A.2.1), and results in a corresponding loss of iodate, and vice versa (Equation A.2.2).

Two mechanisms for the oxidation of iodide to iodate are explored in this paper. In the first, oxidation occurs over a specified timescale, which parameterizes the actual processes involved (Equation A.2.4a). Experiments with the model show that linking oxidation to nitrification in the mixed layer significantly improves the model fit to observations. The production of iodide, driven by the assimilation of carbon, also has an implied link to the nitrogen flux, which can be determined by a Redfield ratio. With oxidation driven by nitrification, the proportion of iodide oxidized to iodate is given by the proportion of nitrogen (in the form of ammonium) that is oxidized to nitrite in the surface ocean layer (Equation A.2.4b).

The tracers iodide and iodate are subject to advection by the monthly mean velocities from the OCCAM ocean general circulation model (Aksenov et al., 2010) (Equations A.2.5–A.2.7), and horizontal and vertical mixing at rates of $K_h = 2{,}000\ \mathrm{m^2\ s^{-1}}$ and $K_z = 1 \times 10^{-4}\ \mathrm{m^2\ s^{-1}}$, respectively. In addition, seasonal mixed layer depth changes result in the exchange of tracers between the upper two model layers and complete mixing of existing and additional tracers in the thickening layer.

A.2 Model Equations

In the mixed layer,

$$\frac{\partial[\mathrm{I^-}]}{\partial t} = PROD_{t\,-\,LAG} \times IC \times F_a \times \frac{1}{MLD} - OXIDATION + TRANSPORT\ , \tag{A.2.1}$$

$$\frac{\partial[\mathrm{IO_3^-}]}{\partial t} = -PROD_{t\,-\,LAG} \times IC \times F_a \times \frac{1}{MLD} + OXIDATION + TRANSPORT, \tag{A.2.2}$$

where *PROD* is the monthly mean production of carbon, *LAG* is the time lag for iodide production from carbon assimilation (60 days), *IC* is the ratio of iodide to carbon production, *MLD* is the seasonally varying mixed layer depth, and

$$F_a = 1 - \exp\left(\frac{-\left[IO_3^-\right]}{\left[IO_{3\ \mathrm{limit}}^-\right]}\right) \tag{A.2.3}$$

is the iodide saturation term, where $IO_3^-{}_{\mathrm{limit}} = 50$ nM.

Oxidation is represented by either a timescale, such that

$$OXIDATION = 1/T_{\mathrm{oxidation}} \times [I^-], \tag{A.2.4a}$$

or is linked to mixed layer nitrification, such that

$$OXIDATION = -REGEN \times PROD_{t\ -\ LAG} \times IC \times F_a \times \frac{1}{MLD}, \tag{A.2.4b}$$

where *REGEN* is the proportion of nitrogen subject to nitrification in the mixed layer (Yool et al., 2007).

The transport of iodide and iodate (represented by tracer *T*) is given by

$$TRANSPORT = u\frac{\partial T}{\partial x} + v\frac{\partial T}{\partial y} + w\frac{\partial T}{\partial z} + K_h\left[\frac{\partial^2 T}{\partial x^2} + \frac{\partial^2 T}{\partial y^2}\right] + K_z\frac{\partial^2 T}{\partial z^2}, \tag{A.2.5}$$

where *u*, *v*, and *w* are the layer-dependent zonal, meridional, and vertical velocities.

Below the mixed layer, there is no production or oxidation of iodide, with changes in iodide and iodate being driven by advection and mixing (Equations A.2.6 and A.2.7).

$$\frac{\partial[I^-]}{\partial t} = TRANSPORT, \tag{A.2.6}$$

$$\frac{\partial\left[IO_3^-\right]}{\partial t} = \ TRANSPORT. \tag{A.2.7}$$

In the deep ocean, iodide and iodate are assumed to have concentrations of 0 and 500 nM, respectively (Chance et al., 2014), and upward advection transports iodide and iodate with these concentrations into the bottom model layer (Figure 1).

Each model simulation was run for 100 years, which allowed iodide and iodate concentrations to reach an equilibrium.

Conflict of Interest

The authors have no financial conflicts of interest with the research in this paper.

Data Availability Statement

The iodine observational data used for this research are available from the British Oceanographic Data Centre (BODC) (Chance et al., 2019b).

Acknowledgments
This research was funded under the Natural Environment Research Council (NERC) Grant NE/N01054X/1. The authors would like to thank Andrew Yool for supplying the data for quantifying mixed layer nitrification from Yool et al. (2007), Alex Baker for the use of his unpublished data (included in Chance et al., 2019a, 2019b), Peter Croot and Kathrin Wuttig for data now included in Chance et al. (2019a, 2019b), and Tomás Sherwen, for providing surface iodide fields derived from a machine learning algorithm. We would like to thank an anonymous reviewer for suggesting improvements to the manuscript.

References

Aksenov, Y., Bacon, S., Coward, A. C., & Nurser, A. J. G. (2010). The North Atlantic inflow to the Arctic Ocean: High-resolution model study. *Journal of Marine Systems*, *79*(1-2), 1–22. https://doi.org/10.1016/j.jmarsys.2009.05.003

Alvain, S., Moulin, C., Dandonneau, Y., & Loisel, H. (2008). Seasonal distribution and succession of dominant phytoplankton groups in the global ocean: A satellite view. *Global Biogeochemical Cycles*, *22*, GB3001. https://doi.org/10.1029/2007GB003154

Amachi, S., Kasahara, M., Fujii, T., Shinoyama, H., Hanada, S., Kamagata, Y., et al. (2004). Radioactive experiments on biological volatilization of organic iodine from coastal seawaters. *Geomicrobiology Journal*, *21*(7), 481–488. https://doi.org/10.1080/01490450490550620 1

Amachi, S., Muramatsu, Y., Akiyama, Y., Miyazaki, K., Yoshiki, S., Hanada S., et al. (2005). Isolation of iodide-oxidising bacteria from iodide-rich natural gas brines and seawaters. *Microbial Ecology*, *49*(4), 547–557. https://doi.org/10.1007/s00248-004-0056-0

Becker, J. J., Sandwell, D. T., Smith, W. H. F., Braud, J., Binder, B., Depner, J., et al. (2009). Global bathymetry and elevation data at 30arc seconds resolution: SRTM30 PLUS. *Marine Geodesy*, *32*(4), 355–371. https://doi.org/10.1080/01490410903297766

Behrenfeld, M. J., & Falkowski, P. G. (1997). Photosynthetic rates derived from satellite-based chlorophyll concentration. *Limnology and Oceanography*, *42*(1), 1–20. https://doi.org/10.4319/lo.1997.42.1.0001

Beman, J. M., Chow, C.-E., King, A. L., Feng, Y., Fuhrman, J. A., Andersson, A., et al. (2011). Global declines in oceanic nitrification rates as a consequence of ocean acidification. *Proceedings of the National Academy of Sciences*, *108*(1), 208–213. https://doi.org/10.1073/pnas.1011053108

Bluhm, K., Croot, P., Wuttig, K., & Lochte, K. (2010). Transformation of iodate to iodide in marine phytoplankton driven by cell senescence. *Aquatic Biology*, *11*(1), 1–15. https://doi.org/10.3354/ab00284

Bluhm, K., Croot, P. L., Huhn, O., Rohardt, G., & Lochte, K. (2011). Distribution of iodide and iodate in the Atlantic sector of the Southern Ocean during austral summer. *Deep-Sea Research Part II: Topical Studies in Oceanography*, *58*(25-26), 2733–2748. https://doi.org/10.1016/j.dsr2.2011.02.002

Campos, M. L. A. M., Farrenkopf, A. M., Jickells, T. D., & Luther, G. W. (1996). A comparison of dissolved iodine cycling at the Bermuda Atlantic Time-series Station and Hawaii Ocean Time-series Station. *Deep-Sea Research Part II: Topical Studies in Oceanography*, *43*(2-3), 455–466. https://doi.org/10.1016/0967-0645(95)00100-X

Campos, M. L. A. M., Sanders, R. J., & Jickells, T. D. (1999). The dissolved iodate and iodide distribution in the South Atlantic from the Weddell Sea to Brazil. *Marine Chemistry*, *65*(3-4), 167–175. https://doi.org/10.1016/S0304-4203(98)00094-02

Carpenter, L. J., Shaw, M. D., Parthipan, R., Wilson, J., MacDonald, S. M., Kumar, R., et al. (2013). Atmospheric iodine levels influenced by sea surface emissions of inorganic iodine. *Nature Geoscience*, *6*(2), 108–111, ISSN 1752-0894. https://doi.org/10.1038/ngeo1687

Chance, R., Baker, A. R., Carpenter, L., & Jickells, T. D. (2014). The distribution of iodide at the sea surface. *Environmental Science: Processes & Impacts*, *16*(8), 1841–1859. https://doi.org/10.1039/C4EM00139G

Chance, R., Malin, G., Jickells, T. D., & Baker, A. R. (2007). Reduction of iodate to iodide by cold water diatom cultures. *Marine Chemistry*, *105*(1-2), 169–180. https://doi.org/10.1016/j.marchem.2006.06.008

Chance, R., Tinel, L., Sherwen, T., Baker, A. R., Bell, T., Brindle, J., et al. (2019a). Global sea-surface iodide observations, 1967–2018. *Scientific Data*, *6*(1), 286. https://doi.org/10.1038/s41597-019-0288-y

Chance R., Tinel, L., Sherwen, T., Baker, A. R., Bell, T., Brindle, J. et al. (2019b). Global sea-surface iodide observations, 1967-2018. British Oceanographic Data Centre - Natural Environment Research Council, UK.

Chance, R., Weston, K., Baker, A. R., Hughes, C., Malin, G., Carpenter, L., et al. (2010). Seasonal and interannual variation of dissolved iodine speciation at a coastal Antarctic site. *Marine Chemistry*, *118*(3-4), 171–181. https://doi.org/10.1016/j.marchem.2009.11.009

de la Cuesta, J. L., & Manley, S. L. (2009). Iodine assimilation by marine diatoms and other phytoplankton in nitrate-replete conditions. *Limnology and Oceanography*, *54*(5), 1653–1664. https://doi.org/10.4319/lo.2009.54.5.1653

Ducklow, H. W., Stukel, M. R., Eveleth, R., Doney, S. C., Jickells, T. D., Scofield, O., et al. (2018). Spring–summer net community production, new production, particle export and related water column biogeochemical processes in the marginal sea ice zone of the Western Antarctic Peninsula 2012–2014. *Philosophical Transactions of the Royal Society A—Mathematical Physical and Engineering Sciences*, *376*(2122), 20170177. https://doi.org/10.1098/rsta.2017.0177

Edwards, A., & Truesdale, V. W. (1997). Regeneration of inorganic iodine species in Loch Etive, a natural leaky incubator. *Estuarine Coastal and Shelf Science*, *45*, 357–366. https://doi.org/10.1006/ecss.1996.0185

Elderfield, H., & Truesdale, V. W. (1980). On the biophilic nature of iodine in seawater. *Earth and Planetary Science Letters*, *50*(1), 105–114. https://doi.org/10.1016/0012-821X(80)90122-3

Fuse, H., Inoue, H., Murakami, K., Takimura, O., & Yamaoka, Y. (2003). Production of free and organic iodine by *Roseovarius* spp. *FEMS Microbiological Letters*, *229*(2), 189–194. https://doi.org/10.1016/S0378-1097(03)00839-5

Ganzeveld, L., Helmig, D., Fairall, C. W., Hare, J., & Pozzer, A. (2009). Atmosphere-ocean ozone exchange: A global modeling study of biogeochemical, atmospheric, and waterside turbulence dependencies. *Global Biogeochemical Cycles*, *23*, GB4021. https://doi.org/10.1029/2008GB003301

Gozlan, R. S. (1968). Isolation of iodine-producing bacteria from aquaria. *Antonie Van Leeuwenhoek*, *34*(1), 226–226. https://doi.org/10.1007/BF02046433

Hardacre, C., Wild, O., & Emberson, L. (2015). An evaluation of ozone dry deposition in global scale chemistry climate models. *Atmospheric Chemistry and Physics*, *15*(11), 6419–6436. https://doi.org/10.5194/acp-15-6419-2015

Hepach, H., Hughes, C., Hogg, K., Collings, S., & Chance, R. (2019). Common features of iodate to iodide reduction amongst a diverse range of marine phytoplankton. *Biogeosciences Discuss*. https://doi.org/10.5194/bg-2019-443

Hung, C.-C., Wong, G. T. F., & Dunstan, W. M. (2005). Iodate reduction activity in nitrate reductase extracts from marine phytoplankton. *Bulletin of Marine Science*, *76*, 61–72.

Jickells, T. D., Boyd, S. S., & Knap, A. H. (1988). Iodine cycling in the Sargasso Sea and the Bermuda inshore waters. *Marine Chemistry*, *24*(1), 61–82. https://doi.org/10.1016/0304-4203(88)90006-0

Long, A., Dang, A., Xiao, H., & Yu, X. (2015). The summer distribution of dissolved inorganic iodine along 18°N in the South China Sea. *Journal of Marine Science: Research & Development*, *05*(03), 169. https://doi.org/10.4172/2155-9910.1000169

Lu, Z., Hoogakker, B. A. A., Hillenbrand, C.-D., Zhou, X., Thomas, E., Gutchess, K. M., et al. (2016). Oxygen depletion recorded in upper waters of the glacial Southern Ocean. *Nature Communications*, *7*(1), 11146. https://doi.org/10.1038/ncomms11146

Luhar, A. K., Woodhouse, M. T., & Galbally, I. E. (2018). A revised global ozone dry deposition estimate based on a new two-layer parameterisation for air-sea exchange and the multi-year MACC composition reanalysis. *Atmospheric Chemistry and Physics*, *18*(6), 4329–4348. https://doi.org/10.5194/acp-18-4329-2018

Luther, G. W., Ferdelman, T., Culberson, C. H., Kostka, J., & Wu, J. F. (1991). Iodine chemistry in the water column of the Chesapeake Bay: Evidence for organic iodine forms. *Estuarine, Coastal and Shelf Science*, *32*(3), 267–279. https://doi.org/10.1016/0272-7714(91)90020-C

Luther, G. W., Wu, J. F., & Cullen, J. B. (1995). Redox chemistry of iodine in seawater: Frontier molecular orbital theory considerations. *Aquatic Chemistry, Advances in Chemistry*, *244*, 135–155. https://doi.org/10.1021/ba-1995-0244.ch006

MacDonald, S. M., Martin, J. C. G., Chance, R., Warriner, S., Saiz-Lopez, A., Carpenter, L., & Plane, J. M. C. (2014). A laboratory characterisation of inorganic iodine emissions from the sea surface: Dependence on oceanic variables and parameterisation for global modelling. *Atmospheric Chemistry and Physics*, *14*(11), 5841–5852. https://doi.org/10.5194/acp-14-5841-2014

Mahajan, A. S., Plane, J. M. C., Oetjen, H., Mendes, L., Saunders, R. W., Saiz-Lopez, A., et al. (2010). Measurement and modelling of tropospheric reactive halogen species over the tropical Atlantic Ocean. *Atmospheric Chemistry and Physics*, *10*(10), 4611–4624. https://doi.org/10.5194/acp-10-4611-2010

Monterey, G. & Levitus, S. (1997). Seasonal variability of mixed layer depth for the world ocean, NOAA Atlas NESDIS 14 U.S. Gov. Printing Office, Wash., D. D., 96 pp. 87.

Moore, C. M., Mills, M. M., Arrigo, K. R., Berman-Frank, I., Bopp, L., Boyd, P. W., et al. (2013). Processes and patterns of ocean nutrient limitation. *Nature Geoscience*, *6*(9), 701–710. https://doi.org/10.1038/NGEO1765

Moore, R. M., & Zafiriou, O. C. (1994). Photochemical production of methyl iodide in seawater. *Journal of Geophysical Research*, *99*(D8), 16,415–16,420. https://doi.org/10.1029/94JD00786

Saiz-Lopez, A., Fernandez, R. P., Ordóñez, C., Kinnison, D. E., Gómez Martín, J. C., Lamarque, J.-F., & Tilmes, S. (2014). Iodine chemistry in the troposphere and its effect on ozone. *Atmospheric Chemistry and Physics*, *14*(23), 13,119–13,143. https://doi.org/10.5194/acp-14-13119-2014

Sarwar, G., Foley, K., Mathur, R., Simon, H., Xing, J. & Fahey, K. (2016). Halogen chemistry in the CMAQ model, 15th Annual CMAS Conference, Chapel Hill, NC, October 24–26.

Sherwen, T., Chance, R. J., Tinel, L., Ellis, D., Evans, M. J., & Carpenter, L. J. (2019a). A machine learning based global sea-surface iodide distribution. *Earth System Science Data*, *11*(3), 1239–1262. https://doi.org/10.5194/essd-11-1239-2019

Sherwen, T., Chance, R. J., Tinel, L., Ellis, D., Evans, M. J., & Carpenter, L. J. (2019b). Global predicted sea-surface iodide concentrations v0.0.1. Centre for Environmental Data Analysis, 30 April 2019. doi:10.5285/6448e7c92d4e48188533432f6b26fe22

Sherwen, T., Evans, M. J., Carpenter, L. J., Andrews, S. J., Lidster, R. T., Dix, B., et al. (2016). Iodine's impact on tropospheric oxidants: A global model study in GEOS-Chem. *Atmospheric Chemistry and Physics*, *16*(2), 1161–1186. https://doi.org/10.5194/acp-16-1161-2016

Sherwen, T., Schmidt, J. A., Evans, M. J., Carpenter, L. J., Großmann, K., Eastham, S. D., et al. (2016). Global impacts of tropospheric halogens (Cl, Br, I) on oxidants and composition in GEOS-Chem. *Atmospheric Chemistry and Physics*, *16*(18), 12,239–12,271. https://doi.org/10.5194/acp-16-12239-2016

Stammler, I., Rothe, M., Hense, I., & Hepach, H. (2013). Numerical modelling of methyl iodide in the eastern tropical Atlantic. *Biogeosciences*, *10*(6), 4211–4225. https://doi.org/10.5194/bg-10-4211-2013

Stroeve, J., & Meier, W. N. (2018). Sea ice trends and climatologies from SMMR and SSM/I-SSMIS, version 3. Boulder, Colorado USA. NASA National Snow and Ice Data Center Distributed Active Archive Center, https://doi.org/10.5067/IJ0T7HFHB9Y6

Tian, R. C., Marty, J. C., Nicolas, E., Chiaverini, J., Ruiz-Pino, D., & Pizay, M. D. (1996). Iodine speciation: A potential indicator to evaluate new production versus regenerated production. *Deep-Sea Research Part I*, *43*(5), 723–738. https://doi.org/10.1016/0967-0637(96)00023-4

Truesdale, V. W., Bale, A. J., & Woodward, E. M. S. (2000). The meridional distribution of dissolved iodine in near-surface waters of the Atlantic Ocean. *Progress in Oceanography*, *45*(3-4), 387–400. https://doi.org/10.1016/S0079-6611(00)00009-4

Truesdale, V. W., Danielssen, D. S., & Waite, T. J. (2003). Summer and winter distributions of dissolved iodine in the Skagerrak. *Estuarine, Coastal and Shelf Science*, *57*(4), 701–713. https://doi.org/10.1016/S0272-7714(02)00412-2

Truesdale, V. W., Watts, S. F., & Rendell, A. R. (2001). On the possibility of iodide oxidation in the near-surface of the Black Sea and its implications to iodine in the general ocean. *Deep-Sea Research*, *48*(11), 2397–2412. https://doi.org/10.1016/S0967-0637(01)00021-8

Tsunogai, S. (1971). Iodine in the deep water of the ocean. *Deep Sea Research and Oceanographic Abstracts*, *18*(9), 913–919. https://doi.org/10.1016/0011-7471(71)90065-9

Waite, T. J., & Truesdale, V. W. (2003). Iodate reduction by *Isochrysis galbana* is relatively insensitive to de-activation of nitrate reductase activity—Are phytoplankton really responsible for iodate reduction in seawater? *Marine Chemistry*, *81*(3-4), 137–148. https://doi.org/10.1016/S0304-4203(03)00013-6

Waite, T. J., Truesdale, V. W., & Olafsson, J. (2006). The distribution of dissolved inorganic iodine in the seas around Iceland. *Marine Chemistry*, *101*(1-2), 54–67. https://doi.org/10.1016/j.marchem.2006.01.003

Wessel, S., Aoki, S., Winkler, S., Weller, R., Herber, A., & Gernandt, H. (1998). Tropospheric ozone depletion in polar regions: A comparison of observations in the Arctic and Antarctic. *Tellus*, *50*(1), 34–50. https://doi.org/10.3402/tellusb.v50i1.16020

Wong, G. T. F. (1991). The marine geochemistry of iodine. *Reviews in Aquatic Sciences*, *4*, 45–73.

Wong, G. T. F. (2001). Coupling iodine speciation to primary, regenerated or "new" production: A re-evaluation. *Deep-Sea Research Part I*, *48*(6), 1459–1476. https://doi.org/10.1016/S0967-0637(00)00097-2

Wong, G. T. F., Plumsomboon, A. U., & Dunstan, W. M. (2002). The transformation of iodate to iodide in marine phytoplankton cultures. *Marine Ecology Progress Series*, *237*, 27–39. https://doi.org/10.3354/meps237027

Yool, A., Martin, A. P., Fernandez, C., & Clark, D. R. (2007). The significance of nitrification for oceanic new production. *Nature*, *447*(7147), 999–1002. https://doi.org/10.1038/nature05885

Zhou, X., Thomas, E., Winguth, A. M. E., Ridgwell, A., Scher, H., Hoogakker, B. A. A., et al. (2016). Expanded oxygen minimum zones during the late Paleocene-early Eocene: Hints from multiproxy comparison and ocean modelling. *Paleoceanography*, *31*, 1532–1546. https://doi.org/10.1002/2016PA003020

Žic, V., & Branica, M. (2006). The distributions of iodate and iodide in Rogoznica Lake (East Adriatic Coast). *Estuarine, Coastal and Shelf Science*, *66*(1-2), 55–66. https://doi.org/10.1016/j.ecss.2005.07.022

Zic, V., Caric, M., & Ciglenecki, I. (2013). The impact of natural water column mixing on iodine and nutrient speciation in a eutrophic anchialine pond (Rogoznica Lake, Croatia). *Estuarine, Coastal and Shelf Science*, *133*, 260–272. https://doi.org/10.1016/j.ecss.2013.09.008